

# Silicon-Dioxide Waveguides With Low Birefringence

L. Grave de Peralta, Ayrton A. Bernussi, H. Temkin, Marcus M. Borhani, *Senior Member, IEEE*, and David E. Doucette

**Abstract**—We describe the use of highly boron-doped silicon dioxide for the preparation of optical waveguides with very low birefringence. Plasma-enhanced chemical vapor deposition was used to vary the boron content from 5 wt% to 10 wt%, at a constant phosphorus content of 4.8%. A transition from compressive to tensile stress was observed at a boron concentration of 9.1%. Pedestal-type waveguides formed with the high-boron top cladding layer show low loss of 0.02 dB/cm. Arrayed waveguide grating devices with a polarization-dependent wavelength shift of 0.01 nm and excellent stability have been demonstrated.

**Index Terms**—Glass, multiplexing, optical waveguides, photoelasticity, polarization.

## I. INTRODUCTION

THE PROBLEM of birefringence in optical waveguides used in wavelength multiplexing devices has received considerable attention and a number of approaches have been attempted to mitigate its effects. The methods used vary from the use of silica substrates, instead of silicon [1], introduction of highly doped glasses [1]–[3], addition of compensating layers [4], and post-deposition ultraviolet irradiation treatment [5]. Modifications of device design, in form of a birefringence-compensating region [6], insertion of a halfwave-plate [7] or stress relief grooves [8] have also been described for the purpose of limiting polarization sensitivity. The possibility of materials-based solution to the birefringence problem would be particularly attractive, but very little detailed information on the properties of highly doped glasses is available.

A variety of integrated optics devices are based on single mode waveguides formed in silicon dioxide ( $\text{SiO}_2$ ) [9]. A typical waveguide, illustrated in Fig. 1(a), consists of three layers of  $\text{SiO}_2$ , each doped to produce the desired index of refraction and reflow properties, deposited and patterned on a silicon substrate. The lower cladding layer, 10–15  $\mu\text{m}$  thick, consisted of undoped  $\text{SiO}_2$  prepared by high-pressure thermal oxidation of silicon. This process forms the oxide on both sides of the Si substrate and the resulting wafer remains flat. The core layer is typically 5  $\mu\text{m}$  thick and it is etched to produce 5–6- $\mu\text{m}$ -wide stripes in order to assure single-mode operation. This layer is doped with phosphorus (P) to increase its index of refraction by 0.01 to 0.014 over that of the undoped  $\text{SiO}_2$ . The upper cladding layer, deposited over the patterned and etched core layer, has a

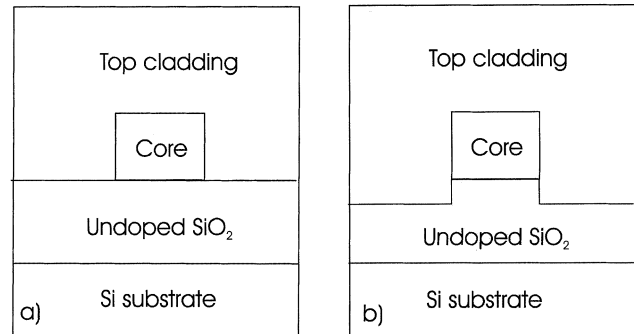


Fig. 1. Schematic cross-section of waveguide structures described here. (a) Conventional single-mode structure. (b) Low birefringence pedestal structures.

thickness of 10–15  $\mu\text{m}$ , and is typically doped with Boron (B) and P to have an index of refraction close to that of the lower cladding layer. The addition of boron lowers the softening temperature of the glass and modifies its reflow properties, in order to provide complete coverage of the etched core layer. Another version of the waveguide structure discussed here is illustrated in Fig. 1(b). All the layer thicknesses are the same as in the conventional waveguide but the core layer is over-etched, by about 2  $\mu\text{m}$ , forming a pedestal-like step in the lower cladding layer, under the remaining core layer. This results in a structure in which the upper cladding layer surrounds the core more completely. A similar approach was previously applied in the fabrication of polarization insensitive phased-array wavelength demultiplexers based on InP ridge waveguides [10]. We show that the pedestal structure, combined with an appropriate level of B in the cladding layer, results in waveguides with very low stress and birefringence.

## II. GLASSES: FABRICATION

The difference in thermal expansion coefficients between the Si substrate and  $\text{SiO}_2$  layers gives rise to compressive biaxial strain in the core and cladding layers. The resulting anisotropic index of refraction introduces a difference in the propagation constants of the transverse electric (TE)- and transverse magnetic (TM)-polarized modes of optical waveguides. In multiplexing devices, this difference shifts the response spectrum between the TE and TM modes of individual channels. The effect of birefringence can be very significant in dense wavelength division multiplexing (WDM) devices where the channel separation may be smaller than 0.4 nm.

Thermal expansion coefficient of bulk glasses ( $\text{SiO}_2$ ) is known to be a strong function of the boron concentration [11]. For instance, in borosilicate glass the thermal expansion

Manuscript received October 3, 2002; revised February 28, 2003. This work was supported by the Jack F. Maddox Foundation, State of Texas, under the TDT program, and by Texas Instruments.

L. G. de Peralta, A. A. Bernussi, and H. Temkin are with the Nano Tech Center, Texas Tech University, Lubbock, TX 79409 USA.

M. M. Borhani and D. E. Doucette are with X-Fab Texas, Lubbock, TX 79415 USA.

Digital Object Identifier 10.1109/JQE.2003.813194

coefficient increases linearly from a low  $7 \times 10^{-7}/^{\circ}\text{C}$  to a high  $28 \times 10^{-7}/^{\circ}\text{C}$  as the boron content (in weight%) is increased from 2% to 13%. At a boron concentration of 11.5%, the room-temperature thermal expansion coefficient of the B-doped glass matches that of Si. The upper cladding layer of a waveguide fabricated with such a glass would not strain the core layer and thus result in low birefringence. Its index would be lowered by the large boron content and phosphorous would have to be added to increase the index to the desired value. The addition of phosphorus increases the thermal expansion coefficient, at approximately the same rate as that of the boron, limiting the amount that can be introduced. It is believed that the B and P content achievable in thin-film glasses is quite limited. For example, upper cladding layer doping of only 2.5% P and 4% B is used to produce, by low-pressure chemical vapor deposition (LPCVD), the desired index of refraction and reflow properties [5] but this glass composition results in high birefringence. The thermally induced compressive stress in  $\text{SiO}_2$  with this B and P content may be as high as  $-(75\text{--}90)$  MPa, resulting in high birefringence-induced splitting between the TE and TM waveguide modes of  $\sim 0.2$  nm.

There are two primary methods of  $\text{SiO}_2$  deposition used in the fabrication of optical waveguide devices, flame hydrolysis deposition (FHD) [12], and LPCVD [9]. The low-temperature FHD deposition is capable of producing highly doped layers of  $\text{SiO}_2$ , where the dopants are Germanium, B, and P, that can be converted to high-quality glass in a high-temperature sintering process. The LPCVD process used for many years for the deposition of upper cladding layers of optical waveguides is a high temperature process (over  $600^{\circ}\text{C}$ ) that relies on a reaction of tetraethylorthosilane and ammonia, known as TEOS. The high deposition temperature limits dopant incorporation, especially B, to few percent. The TEOS process is commonly used in the silicon industry and advanced deposition methods have been developed for the metal-oxide-semiconductor (MOS) process. One of these, plasma enhanced chemical vapor deposition (PECVD), can be carried out at low temperatures ( $400^{\circ}\text{C}$ – $450^{\circ}\text{C}$ ) and it allows for the incorporation of considerably higher B fractions than those possible with LPCVD. We show here that the PECVD process can be used to prepare layers of  $\text{SiO}_2$  with the B and P content needed to match the thermal expansion coefficient of Si and to adjust the index of refraction to form high quality waveguides. We also use the PECVD TEOS process for the preparation of P-doped core layers with low optical losses.

The core and top cladding layers of  $\text{SiO}_2$  used in this work were TEOS based and deposited by PECVD using commercial silicon-grade equipment (Applied Materials P5000) on 150-mm-diameter silicon wafers. The B and P dopants were derived from conventional sources of trimethylborate and trimethylphosphate, respectively. Deposition rates of  $\sim 0.3 \mu\text{m}/\text{min}$  were obtained at the susceptor temperature of  $430^{\circ}\text{C}$ . Dopant calibration was based on X-ray fluorescence and infrared-absorption measurements. After deposition layers were annealed at  $920^{\circ}\text{C}$  for 30 min. Wafer stress was determined using a laser-based curvature measurement system with the resolution better than 0.05 MPa. Index and thickness uniformity maps were obtained using automated reflectivity

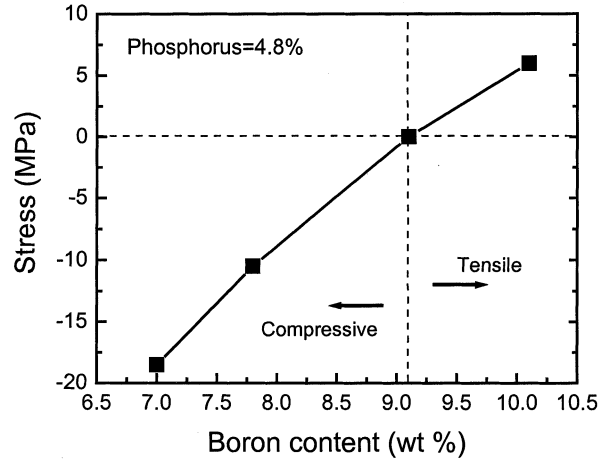


Fig. 2. Stress in  $5\text{-}\mu\text{m}$ -thick BP-TEOS layers plotted as a function of increasing boron content. The phosphorus content was kept constant at 4.8 wt%. Wafers were annealed at  $920^{\circ}\text{C}$  for 30 min.

measurements at  $632.8$  nm. Additional index measurements at  $1.55 \mu\text{m}$  were done using a prism coupler. The on-wafer index and thickness uniformity were controlled to better than 0.01% and 1.5%, respectively. Wafers were free of cracks or bubbles. With high-quality deposition and metrology tools available at the CMOS process line, we were able to reproducibly obtain baseline waveguide losses of  $0.02\text{--}0.03$  dB/cm.

### III. GLASSES: EXPERIMENTAL RESULTS

Results of our PECVD studies are illustrated in Fig. 2. All the layers used were  $5 \mu\text{m}$  thick and their P content was fixed at 4.8%. The B content was varied, in different wafers, from 7% to 11%. The stress was measured after wafer annealing. Increasing B content resulted in reduced compressive stress. The stress approaches zero for a B content of 9.1% and it changes the sign, becomes tensile, for larger B content. At this point the layer is free of stress. Stress induced bowing of the wafer becomes negligibly small allowing for high-resolution photolithography. The compressive-tensile transition is also observed in films with lower P content, at slightly higher B content. Highly B-doped layers with the P content higher than 5% become hazy and B precipitates are observed upon high temperature annealing. The high B levels illustrated in Fig. 2 are apparently close to the solubility limit. While this may give rise to concerns about long-term stability of the high B glass, the annealed wafers appear completely stable. This is illustrated below with temperature cycling experiments carried out on arrayed waveguide grating (AWG) devices [13] fabricated with the high-B glass in the cladding layer.

The ability to produce low stress glass and even to change the sign of the stress is crucial to the design and preparation of optical waveguides with low birefringence. However, the index of refraction of the high-B high-P layers is  $\sim 1.45$ , measured at a wavelength of  $1.55 \mu\text{m}$ , larger than the  $\sim 1.44$  desired for waveguides based on P-doped core layer. Fig. 3 shows changes in index of refraction with P concentration, measured at  $1.55 \mu\text{m}$ , at a fixed B content of 9.1%. The index of refraction varied from  $n = 1.442$  to slightly over 1.45 as the phosphorus content was

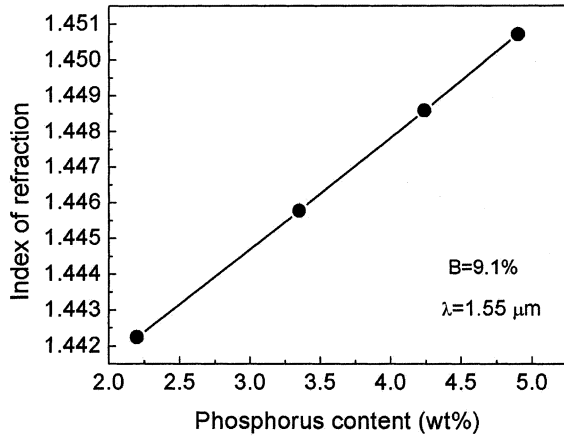


Fig. 3. Dependence of the index of refraction, measured at a wavelength of 1.55  $\mu\text{m}$ , on the phosphorus content of 5- $\mu\text{m}$ -thick BP-TEOS layers. The boron content was fixed at 9.1 wt%.

TABLE I  
MATERIAL PARAMETERS OF SILICON AND SILICON-DIOXIDE GLASSES

Material	E ( $\times 10^{10}\text{N/m}^2$ )	$\nu$	$\alpha$ ( $\times 10^{-7}/^\circ\text{C}$ )	n	P <sub>11</sub>	P <sub>12</sub>
Si <sup>(a)</sup>	15	0.28	38*			
Core glass (P-TEOS)	8	0.2	30	1.456	0.121	0.270
Undoped SiO <sub>2</sub> <sup>(b)</sup>	7.29	0.17	4.6	1.446	0.121	0.270
Low-B SiO <sub>2</sub>	8	0.2	28	1.446	0.121	0.270
High-B SiO <sub>2</sub>	8	0.2	38	1.446	0.121	0.270

\*Average value of the thermal expansion coefficient  $\alpha$  in the temperature range 25  $^\circ\text{C}$ –800  $^\circ\text{C}$ –1

(a) Ref. [16].

(b) Ref. [11].

changed from  $\sim 2\%$  to  $\sim 5\%$ . Increased P content in the B- and P-doped layer increases the index, as expected. In contrast, increased B content decreases the index. For glasses with the B content of 9%–10% the desired index value is reached for the P content between 2.5% and 3.5%. As dopant concentrations are lowered, biaxial stress increases resulting in a lower limit on the useful concentrations of B and P.

#### IV. MODELING AND DISCUSSION

The reduced stress in the upper cladding layer has a large effect on the magnitude of stress and its distribution in the core layer and its vicinity. This was calculated using the two-dimensional plane strain approximation and the finite-element method described by Okamoto [14], using the parameters listed in Table I. It was assumed that above the glass softening point of  $\sim 800$   $^\circ\text{C}$ , there is no stress in the core or cladding layers. Once the stress distribution was calculated, it could be related to local changes at the point  $(i, j)$  in the refractive index through the following expressions [14]:

$$\Delta n_x(i, j) = -C_1\sigma_x(i, j) - C_2[\sigma_y(i, j) + \sigma_z(i, j)] \quad (x \text{ polarization})$$

$$\Delta n_y(i, j) = -C_1\sigma_y(i, j) - C_2[\sigma_x(i, j) + \sigma_z(i, j)] \quad (y \text{ polarization}). \quad (1)$$

Here,  $\sigma_x$  and  $\sigma_y$  are the stress components in the directions parallel and perpendicular to the wafer, respectively, and  $\sigma_z$  is the stress component in the propagation direction. The local birefringence ( $\Delta n_{i,j} = \Delta n_x(i, j) - \Delta n_y(i, j)$ ) is proportional to the local stress difference in the parallel and perpendicular directions ( $\sigma_x(i, j) - \sigma_y(i, j)$ ).

The photoelastic constants  $C_1$  and  $C_2$  are related to the Pockels coefficient  $P_{11}$  and  $P_{12}$  by [14]

$$C_1 = \frac{n^3}{2E}(P_{11} - 2\nu P_{12}), \quad C_2 = \frac{n^3}{2E}[-\nu P_{11} + (1 - \nu)P_{12}] \quad (2)$$

where  $E$  is the Young's modulus of the glass and  $\nu$  is the Poisson's ratio. In order to determine the photoelastic constants  $C_1$  and  $C_2$ , we used the Pockels coefficients of the undoped SiO<sub>2</sub> for all the glasses [15]. The values of the parameters  $E$  and  $\nu$  were obtained experimentally for each glass.

The effective birefringence  $\Delta n$  is calculated as a weighted sum of the local contributions  $\Delta n_{i,j}$  [14]

$$\Delta n = \sum_{ij} w_{ij} \Delta n_{ij}, \quad w_{ij} = \frac{I_{ij}}{\sum_{ij} I_{ij}} \quad (3)$$

where  $I_{ij}$  is the local light intensity. Light distribution in the waveguide, including cladding layers, was calculated using a beam-propagation method. Since the cladding region contains a significant portion of the TE and TM mode intensity, their contribution to the waveguide birefringence is important.

Fig. 4 shows the distribution of the product of stress-induced local index change and the normalized local light intensity  $w_{ij}\Delta n_{ij}$  in the standard and pedestal-type waveguides. In both cases, the upper cladding layer is formed of high-B glass under a slight tensile stress. In the standard waveguide, shown in Fig. 4(a), all the index changes in the lower cladding layer are positive. The largest contribution is in the region under the core. This is the result of the compressive strain of undoped oxide of the lower cladding layer. Positive index changes are also calculated at the sides of the core region. Negative index changes are calculated above the core region and in the core itself. In the center of the core, we calculate  $w_{ij}\Delta n_{ij} = -4.98 \times 10^{-9}$ . The largest contribution occurs on either side of the center. Going from the center of the core to the edge,  $w_{ij}\Delta n_{ij}$  increases and then changes the sign at the edge of the core region. Since the birefringence is the sum of local values of  $w_{ij}\Delta n_{ij}$ , given by 3, the presence of negative and positive contributions in the core and its vicinity contributes to low birefringence. In addition, the local values of  $w_{ij}\Delta n_{ij}$  are small, reflecting low stress in the top cladding layer. The calculated birefringence  $\Delta n \sim 17 \times 10^{-5}$  for this case is indeed very small. In waveguides fabricated with conventional low-B glass, we calculate much larger center  $w_{ij}\Delta n_{ij} \sim +3.96 \times 10^{-8}$ . Furthermore, in this case, all the local contributions  $w_{ij}\Delta n_{ij}$  in the core and its vicinity are positive, reflecting large compressive strain of the cladding layer, resulting in a larger  $\Delta n \sim 25 \times 10^{-5}$ . Introduction of

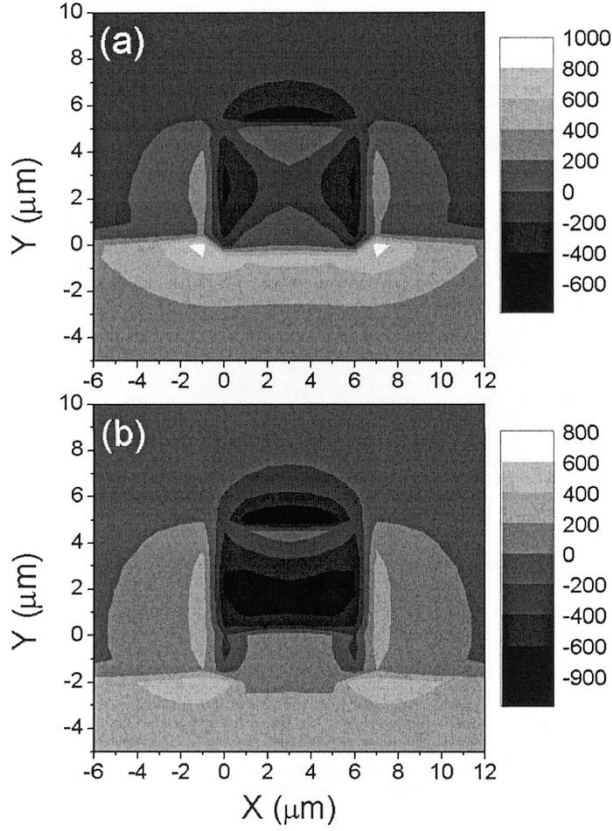


Fig. 4. Distribution of the product of stress induced local index change and the normalized local light intensity  $w_{ij}\Delta n_{ij}$  in (a) standard and (b) pedestal-type waveguides. The gray level scales, shown at the side of each panel, should be multiplied by  $10^{-10}$  to give the real value of  $w_{ij}\Delta n_{ij}$ . The center of the core region is at  $x = 3.0$  and  $y = 2.5$   $\mu\text{m}$ .

the pedestal, illustrated in Fig. 4(b) has two effects. It changes the distribution of  $w_{ij}\Delta n_{ij}$  and its values. In the center of the core, we calculate a larger negative  $w_{ij}\Delta n_{ij} \sim -5.8 \times 10^{-8}$ . Further away from the core, not shown in Fig. 4(b), positive contributions from the etched off lower cladding region are replaced with negative contributions due to the top cladding. Positive contributions from the region under the core are also reduced. These effects produce a significantly lower birefringence of  $\Delta n \sim 5.5 \times 10^{-5}$ . It should be pointed out that this reduction could not be obtained with low-B cladding, since all the index contributions would be positive.

The relation between  $\Delta n$  and  $\Delta\lambda$  in AWG is [1]

$$\Delta\lambda = \Delta n \frac{\Delta L}{m} = \lambda_o \frac{\Delta n}{n_{\text{wg}}} \quad (4)$$

where  $\Delta L$  is the length difference between consecutive grating waveguides,  $m$  is the order of the AWG,  $n_{\text{wg}}$  is the effective refractive index of the waveguide, and  $\lambda_o$  is the design wavelength. For the low-B structure we calculate  $\Delta\lambda \sim 0.26$  nm. The replacement of the low-B cladding with the high-B material results in a reduced  $\Delta\lambda \sim 0.17$  nm. Finally, the combination of high-B cladding and the pedestal results in  $\Delta\lambda \sim 0.056$  nm. This calculation correctly describes the trend in birefringence and the birefringence values for low-B cladding and the conventional waveguide with high-B cladding. It tends to overestimate the value of  $\Delta\lambda$  in the pedestal-type waveguide, as demonstrated

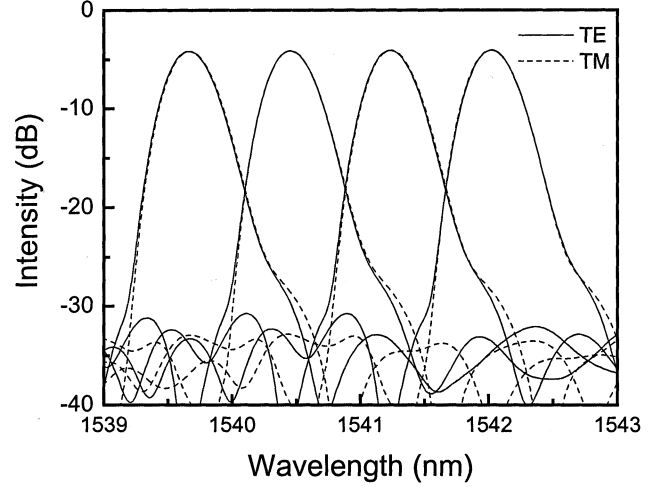


Fig. 5. Polarization response of four channels of an AWG fabricated with high-B top cladding layer. Polarization dependent wavelength shift is smaller than 0.01 nm for all of the 40 channels of this 100-GHz device.

below. We attribute the overestimate to the uncertainties in the parameters used in the simulation.

## V. LOW BIREFRINGENCE AWGS

AWGs constructed using the two types of waveguides illustrated in Fig. 1 were fabricated and their polarization response evaluated and compared to that of a low-B structure. These were 40-channel Gaussian response devices with the channel-to-channel separation of 100 GHz and the 3-dB channel bandwidth of  $\sim 20$  GHz. Fig. 5 shows the wavelength's response of four adjacent channels of a high-B cladding AWG with pedestal-type waveguides. Testing was done by rotating the input polarization from TE to TM and measuring the output response. It is clear that the polarization-dependent wavelength shift (PDW) is extremely small, unmeasurable in some cases. In the channels shown in Fig. 5, the single-channel PDW was 0.00–0.01 nm. The average PDW for all 40 channels of this device was less than 0.01 nm, fairly typical of AWGs formed with high-B glasses and pedestal waveguides. This negligibly small polarization dependence compares well to the best results, 0.02 nm, obtained on AWGs made with highly doped glasses prepared by FHD [1], [3]. The intensity variation resulting from the polarization rotation, polarization-dependent loss (PDL), is negligible in our devices, as shown in Fig. 5. The results obtained for a combination of high-B cladding and pedestal-type waveguide were significantly better than those of low-B devices. With a low-B cladding, in the absence of any birefringence compensation, we measured the wavelength shift of 0.2 nm, in good agreement with our calculations. It should be also pointed out that the use of high-B cladding layer, with or without the pedestal structure, does not increase the insertion loss of the AWG. With either type of waveguide we measure the average insertion loss between 3.3 and 4.5 dB, in different devices.

A thermal cycling experiment demonstrating excellent stability of AWGs prepared using high-B  $\text{SiO}_2$  cladding is shown in Fig. 6. The device was based on a pedestal-type waveguide. It was packaged with an epoxy-attached v-groove fiber array and

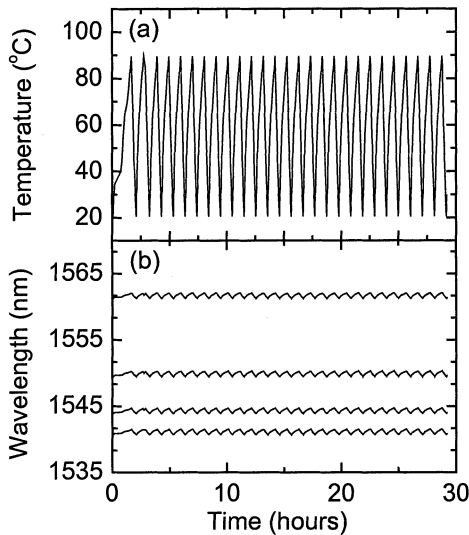


Fig. 6. Stability of AWG response subjected to repeated temperature cycling of 70 °C. (a) Temperature profile. (b) Wavelength response of the four channels.

placed in a thermal cycling oven. The wavelength response of selected channels was continuously monitored. In addition, the polarization response was measured before and after the experiment. The device was subjected to temperature cycles ranging from 20 °C to 90 °C, without any humidity control, as shown in Fig. 6(a). A typical experiment used 27 cycles in a 29-h period. The wavelength response varied with the temperature, as shown in Fig. 6(b) for four different channels, but it did not drift. The shift of  $1.2 \times 10^{-2}$  nm/°C in the wavelength response during the up and down parts of the cycle is due to the normal temperature dependence of the index. Devices subjected to multiple experiments of this type did not show any cumulative changes. No changes in the polarization response were detected, confirming excellent stability of high-B glasses.

## VI. CONCLUSION

We have carried out detailed experiments on plasma enhanced CVD deposition of silicon-dioxide highly doped with boron and phosphorus. A transition from compressive to tensile stress was observed at a boron concentration of 9.1%, for a fixed phosphorus content of 4.8%. Highly doped glass deposited under tensile stress was used as a top cladding layer in optical waveguides, where it compensated for compressive stress of the phosphorus-doped core and the undoped lower cladding layers. This effect is confirmed by experimental results and modeling. Birefringence in the waveguide was simulated by combining calculated stress and optical field intensity distributions. We show that a pedestal-type waveguide results in particularly low birefringence. This was confirmed with results of AWGs with birefringence lower than 0.01 nm. Finally, we show excellent stability of waveguides formed with high-B glasses in temperature cycling experiments.

## ACKNOWLEDGMENT

The authors thank Sevin Rosen Funds, Inc., for making it possible to obtain equipment needed for device evaluation.

## REFERENCES

- [1] S. Suzuki, S. Sumida, Y. Inoue, and Y. Ohmori, "Polarization-insensitive arrayed-waveguide gratings using dopant-rich silica-based glass with thermal expansion adjusted to Si substrate," *Electron. Lett.*, vol. 33, pp. 1173–1174, 1997.
- [2] S. M. Ohja, C. Cureton, T. Bricheno, S. Day, D. Moule, A. J. Bell, and J. Taylor, "Simple method of fabricating polarization insensitive and very low cross-talk AWG grating device," *Electron. Lett.*, vol. 34, pp. 78–79, 1998.
- [3] A. Kilian, J. Kirchhof, B. Kuhlow, G. Przyrembel, and W. Wischmann, "Birefringence free planar optical waveguide made by flame hydrolysis deposition (FHD) through tailoring of the overcladding," *J. Lightwave Technol.*, vol. 18, pp. 193–198, 2000.
- [4] K. Worhoff, B. J. Offrein, P. V. Lambeck, G. L. Bona, and A. Driessen, "Birefringence compensation applying double-core waveguiding structures," *IEEE Photon. Technol. Lett.*, vol. 11, pp. 206–208, 1999.
- [5] B. I. Greene, T. A. Strasser, and C. A. Volkert, "Radiolytic modification of birefringence in silica planar waveguide structures," U.S. Patent 5 506 925, Apr. 9, 1996.
- [6] C. Henry, M. Milbrodt, and H. Yaffe, "Polarization compensated integrated optical filters and multiplexers," U.S. Patent 5 341 444, Aug. 23, 1994.
- [7] Y. Inoue, Y. Ohmori, M. Kawachi, S. Ando, T. Sawada, and H. Takahashi, "Polarization mode converter with polyimide half wave-plate in silica based planar lightwave circuits," *IEEE Photon. Technol. Lett.*, vol. 6, pp. 626–628, 1994.
- [8] M. Kawachi, K. Jingui, N. Takato, M. Yasu, and K. Okamoto, "Single mode channel optical waveguide with a stress-induced birefringence control region," U.S. Patent 4 781 424, Nov. 1, 1988.
- [9] Y. P. Li and C. H. Henry, "Silicon optical bench waveguide technology," in *Opt. Fiber Telecommun.*, vol. IIIB, ch. 8, 0-12-395 171-2.
- [10] H. Bissessur, P. Pagnod-Rossiaux, R. Mestric, and B. Martin, "Extremely small polarization independent phased-array demultiplexers on InP," *IEEE Photon. Technol. Lett.*, vol. 8, pp. 554–556, 1996.
- [11] S. Musikant and B. J. T. Thompson, Eds., *Optical Materials, A Series of Advances*. New York: Marcel Dekker, 1990, vol. 1.
- [12] M. Kawachi, M. Yasu, and T. Edaishi, "Fabrication of SiO<sub>2</sub>-TiO<sub>2</sub> glass planar optical waveguides by flame hydrolysis deposition," *Electron. Lett.*, vol. 19, pp. 583–584, 1983.
- [13] C. Dragone, C. A. Edwards, and R. C. Kistler, "Integrated optics  $N \times N$  multiplexer on silicon," *IEEE Photon. Technol. Lett.*, vol. 3, pp. 896–899, 1991.
- [14] K. Okamoto, *Fundamentals of Optical Waveguides*. New York: Academic, 2000, pp. 264–269.
- [15] J. Xu and R. Stroud, *Acousto-Optic Devices: Principles, Design, and Applications*. New York: Wiley, 1992, p. 583.
- [16] O. Madelung, *Semiconductors-Basic Data*. New York: Springer, 1996, pp. 15–16.

**L. Grave de Peralta** received the M.S. degree in physics from Oriente University, Santiago de Cuba, Cuba, in 1982, and the Ph.D. degree in electrical engineering from Texas Tech University, Lubbock, in 2000.

He was Professor in the Department of Experimental and Theoretical Physics, Oriente University, until 1989. His earlier work focused in VCSEL design and material characterization (luminescence and X-ray reflectivity). Since 2000, he has been working in planar lightwave circuit design and development at Applied WDM Inc., Lubbock, TX, and at Texas Tech University.

**Ayrton A. Bernussi** received the B.S., M.S., and Ph.D. degrees in Physics from Universidade Estadual de Campinas (Unicamp), Campinas, Brazil, in 1981, 1984, and 1990, respectively.

In 1988, he joined the Optoelectronic Group at the Brazilian Telecommunication Company (Telebras), where he was involved in the development of semiconductor lasers and materials. From 1994 to 1995, he was a post-doctoral Researcher at the Electrical Engineering Department, Colorado State University, Fort Collins. His research during this period was on high-temperature properties of strained quantum-well lasers. During 2000–2001, he was with the National Synchrotron Light Laboratory (LNLS), Campinas, Brazil, where he was involved in the development of semiconductor high-power lasers. Since 2001, he is a Senior Research Associate at the Electrical Engineering Department, Texas Tech University, Lubbock, where he is involved in the development, characterization, and packaging of planar lightwave circuits.

**H. Temkin**, photograph and biography not available at the time of publication.

**Marcus M. Borhani** (M'91–SM'01) received the B.S. and M.S. degrees in electrical engineering from Kansas State University (KSU), Manhattan, in 1973 and 1976, respectively.

From 1974 to 1977, he was a Teaching Assistant at KSU, conducting research in the area of ion implantation using the 600-KEV Cockroft Walton accelerator. He joined Texas Instruments' Semiconductor Group in 1977 as a Product Engineer for the 4 K and later 64 K DRAM memory devices. He has management experience in multiprobe, backgrind, and backside metal in the wafer fab, was a Product Engineering Section Manager for several generations of CMOS memory devices, including ROM and EPROM, and has managed test operations and test engineering support for semiconductor devices. He then became Product Engineering Section Manager for several generations of flash EPROM technology. He helped organize the semiconductor foundry for X-Fab Texas, Lubbock, TX, in 1999, where he has been involved in the development of optical devices in the area of WDM.

Dr. Borhani has been a Professional Engineer in Texas since 1991. He is Chair of IEEE South Plains Section and its Reliability Society and a Director of the local chapter of the Texas Society of Professional Engineers (TSPE).

**David E. Doucette** received the B.A. degree in chemistry from Texas Tech University (TTU), Lubbock, in 1994.

He joined Texas Instruments' Semiconductor Group in 1994 as Process Engineer for the Wet Chemical Surface Preparation Process Engineering Group. He has additional experience in thinfilm, diffusion, and SOG wafer fab process integration.

He helped organize the semiconductor foundry for X-Fab Texas, Lubbock, TX, in 1999, where he has been involved in the release, development of Thinfilm dielectric processes for optical devices in the area of WDM.